Crosslinking by ZapD drives the assembly of short, discontinuous FtsZ filaments into ring-like structures in solution

Adrián Merino-Salomón[1], Jonathan Schneider[2,3], Leon Babl[1], Jan-Hagen Krohn[1,4], Marta Sobrinos-Sanguino[5], Tillman Schäfer[6], Juan R. Luque-Ortega[5], Carlos Alfonso[7], Mercedes Jiménez[7], Marion Jasnin[3]*, German Rivas[7]* & Petra Schwille[1]*.

1- Department of Cellular and Molecular Biophysics, Max Planck Institute of Biochemistry, 82152 Martinsried, Germany.
2- Department of Molecular Structural Biology, Max Planck Institute of Biochemistry, 82152 Martinsried, Germany.
3- Helmholtz Pioneer Campus, Helmholtz Zentrum München, 85764 Neuherberg, Germany.
4- Exzellenzcluster ORIGINS, Boltzmannstr. 2, 85748 Garching, Germany.
5- Molecular Interactions Facility, Centro de Investigaciones Biológicas Margarita Salas, Consejo Superior de Investigaciones Científicas (CSIC), 28040 Madrid, Spain.
6- Cryo-EM facility, Max Planck Institute of Biochemistry, 82152 Martinsried, Germany.
7- Centro de Investigaciones Biológicas Margarita Salas, Consejo Superior de Investigaciones Científicas (CSIC), 28040 Madrid, Spain.

Correspondence: marion.jasnin@helmholtz-muenchen.de; rivas@cib.csic.es; schwille@biochem.mpg.de

Abstract

In most bacteria, division depends on a cytoskeletal structure, the FtsZ ring, that functions as a scaffold to recruit additional proteins, with which it forms the machinery responsible for division, the divisome. The detailed architecture of the ring, in particular the mechanisms of assembly, stabilization, and disassembly, are still largely unknown. Here, we highlight the role of FtsZ-associated proteins (Zaps) that stabilize the FtsZ ring by crosslinking the filaments. Among Zap proteins, ZapD binds the C-terminal domain of FtsZ, which serves as a hub for its regulation. We demonstrate that ZapD crosslinks FtsZ filaments into ring-like structures formed by a discontinuous arrangement of short filaments. Using cryo-electron tomography combined with biochemical analysis, we reveal the three-dimensional organization of the ring-like structures and shed light on the mechanism of FtsZ filament crosslinking by ZapD. Together, our data provide a model of how FtsZ-associated proteins can stabilize FtsZ filaments into discontinuous ring-like structures reminiscent of that existing in the bacterial cell.

Introduction

Cell division is mediated in bacteria by a multiprotein complex whose components interact reversibly to form a division ring that drives cytokinesis, the divisome[1–5]. The FtsZ protein, a structural homolog of eukaryotic tubulin with which it shares its GTPase and polymerization activities, is central to this process in most bacteria[6–12]. FtsZ is the main component of the Z-ring, a structure formed at mid-cell during cell division, which provides a scaffold for recruiting other division proteins and is essential for constricting the membrane[13–17]. The initial pathway for ring formation is the GTP-dependent polymerization of FtsZ, which occurs through a conformational switch in the polymer allowing treadmilling of single-stranded filaments[18–25]. In response to environmental conditions, the FtsZ filaments can further assemble into various structures such as bundles, sheets, toroids, or spirals[21,22,26–37].

The molecular components involved in cell division must be in the right place at the right time during the cell cycle. Several factors in this spatiotemporal regulation modulate FtsZ assembly. In *Escherichia coli*, FtsA and ZipA tether FtsZ to the membrane[34,38–43] and, together with a set of FtsZ-associated proteins (Zaps), stabilize the ring[44–51]. Conversely, negative modulators prevent FtsZ assembly at other sites, namely Min proteins at the polar regions[52,53] and SlmA on the nucleoid[54,55]. Most of these modulators interact with FtsZ through its carboxy-terminal end, which acts as a central hub that modulates division assembly[56–58].

To date, a high-resolution structure of the FtsZ ring (Z ring) is still missing. Most data support a discontinuous arrangement of FtsZ filaments distributed in patches along the equatorial circle, and held together by their lateral interactions and interactions with Zap proteins[4,16,59–63]. Cross-linking of filaments by Zap proteins is critical to maintain the juxtaposed organization of filaments into a ring-like structure, which may also be relevant to the functionality of the divisome and to the mechanism of force generation in cytokinesis[1,5,16,19,64–68].

Zap proteins have overlapping functions in stabilizing the Z ring within dividing cells. Individually, they are dispensable for division, exhibiting less compacted Z rings in the absence of individual genes, while co-knock-out of two or more Zaps leads to cell elongation[4,44–47,50,69]. The different Zap proteins share no sequence homology, and their structure and mechanism of FtsZ filament crosslinking differ[46,49,70]. Zap proteins may also participate in the mechanisms of active removal of FtsZ from the septum at the final stage of constriction[71,72] and in guiding the Z ring to the replication terminus region of the chromosome, through interaction with MatP to form the scaffolding anchor called Ter -linkage[73].

ZapD is the only Zap protein known to crosslink FtsZ by binding its C-terminal domain, suggesting a function as a key stabilizer of the Z ring superstructure[45,70,74–78] (Fig. 1a). ZapD is a symmetrical dimer consisting of an α-helical domain and a β-strand domain containing a positively charged binding pocket required for crosslinking and bundling FtsZ filaments[74,78]. ZapD binds to the C-terminal region of FtsZ through electrostatic interactions[78]. ZapD crosslinks FtsZ filaments, promoting bundling and significantly reducing the GTPase activity of FtsZ[45]. The mechanism underlying the bundling of FtsZ filaments is still unknown, although a model of how ZapD crosslinks adjacent FtsZ filaments has been proposed based on the structural analysis of ZapD-FtsZ interactions[74]. In this model, the ZapD dimer connects two FtsZ filaments through the C-terminal domain, which organizes them in an antiparallel orientation (Fig. 1a). However, the experimental validation of this model is still pending. Characterizing how ZapD crosslinks FtsZ filaments can shed light on the molecular mechanism behind Z ring assembly.

Here, we used cryo-electron microscopy (cryo-EM) and cryo-electron tomography (cryo-ET) combined with biochemical and biophysical assays to study the structural organization of FtsZ polymers in the presence of ZapD. This integrated approach revealed that ZapD promotes the assembly of FtsZ filaments into toroidal polymers, which is consistent with the low resolution structure of the Z ring visualized *in vivo*[16,79–81]. Our findings allowed us to propose a molecular mechanism that leads to toroid formation, providing valuable information for understanding the stabilization of the Z ring driven by crosslinking division proteins.

Results

ZapD dimer interacts with FtsZ-GDP oligomers

Before characterizing the interaction between FtsZ and ZapD, we first confirmed the robust dimeric state of ZapD through analytical ultracentrifugation (AUC) (Supplementary Fig. 1a (I) and b), in agreement with previous studies[45,75,76,78]. On the other hand, unpolymerized FtsZ-GDP sedimented as two major species compatible with monomers and dimers, as well as a small amount of other oligomeric species of FtsZ[82] (Supplementary Fig. 1a (II)).

Previous structural studies identified a direct interaction of ZapD through the C-terminal domain or central hub of FtsZ, finding charged residues involved in the interaction[75,78]. To independently confirm these results, we studied the interaction between FtsZ-GDP and ZapD by AUC (Supplementary Fig. 1a (III)). We demonstrated the formation of FtsZ-ZapD complexes that corresponded to a stoichiometry of approximately 2 moles of ZapD per mole of FtsZ (Supplementary Fig. 1a (IV)). In addition, we also confirmed the interaction of both proteins by fluorescence anisotropy and fluorescence correlation spectroscopy (FCS) (Supplementary Fig. 2a and b). In these experiments, an increase in fluorescence anisotropy or diffusion time, respectively, suggests the formation of larger particles as a result of protein-protein interactions.

Thus, we confirmed the interaction between ZapD and unpolymerized FtsZ-GDP, which forms complexes in solution. The AUC results highlight the formation of specific species of FtsZ and ZapD at a molar ratio of approximately 1:2, consistent with the proposed interaction model[74].

ZapD interacts with FtsZ-GTP polymers promoting bundling

ZapD has been suggested to act as a crosslinker of FtsZ filaments promoting bundling in solution[45], although the molecular mechanism of how ZapD crosslinks filaments remains elusive. To decipher the biochemical features underlying the bundling process, we analyzed the formation of large FtsZ macrostructures following interaction with ZapD using light scattering at 350 nm. Neither FtsZ alone nor ZapD alone showed significant light scattering with or without GTP addition. However, ZapD promoted the formation of FtsZ macrostructures upon addition of GTP (Fig. 1b). Increasing concentrations of ZapD showed an increase of light scattering reaching its maximum at molar ratio of about 1:2 (FtsZ:ZapD) (Fig. 1b). In addition, the FtsZ macrostructures disassembled over time. Recurrent replenishment of GTP allowed partial recovery of the light scattering signal, suggesting rapid reassembly of the FtsZ bundles (Supplementary Fig. 3a).

Additionally, ionic strength and pH modulated the interaction of ZapD and FtsZ, also affecting its ability to crosslink FtsZ filaments (Supplementary Fig. 3b and c). The presence of ZapD prior to the addition of GTP did not significantly affect the crosslinking of the filaments (Supplementary Fig. 3d). Interestingly, increasing concentrations of FtsZ at a fixed ZapD concentration did not further promote bundle formation (Supplementary Fig. 3e). This suggests that a certain number of ZapD molecules per FtsZ filament might be required or optimal to crosslink them efficiently. ZapD also decreased the GTPase activity of FtsZ due to filament crosslinking, decreasing it to 30% and reaching 20% at equimolar or higher ZapD concentrations, respectively (Fig. 1c), in agreement with previous studies[45]. Similarly, at higher ionic strength, the bundling effect of ZapD was limited (Supplementary Fig. 3b), favoring less bundle formation and decreased GTPase activity (Supplementary Fig. 4).

These results demonstrate that ZapD dimers can crosslink filaments into dynamic FtsZ bundles that disassemble over time. Lower pH and ionic strength favor bundle assembly, as predicted from the electrostatic nature of the interaction with ZapD[75,78]. At the same time, the bundling effect of ZapD is strongly dependent on the protein ratio used. This highlights the role of the number of ZapD molecules per FtsZ filament in stabilizing the bundle structure, with an optimum at a molar ratio of about 1:1 or 1:2 (FtsZ:ZapD), following the same trend observed with FtsZ-GDP (Supplementary Fig. 1a (IV)).

ZapD promotes the formation of FtsZ toroids

Next, we used cryo-electron microscopy (cryo-EM) to reveal the structure and assembly mechanism of ZapD-mediated FtsZ bundles. Previous studies had visualized regular bundles by negative-stain transmission electron microscopy [45,74,78]; cryo-EM allowed us to avoid any staining artifact. After the addition of GTP, we observed the formation of single and double FtsZ filaments in solution (Fig. 2a). In the presence of ZapD at equimolar or higher concentrations, FtsZ filaments assemble into bundles that form circular toroidal structures (Fig. 2b and c). These toroids have not been observed before for other protein interactions with FtsZ. Toroids coexist with other bundle types, but remain predominant (Fig. 2b, c and Supplementary Fig. 5a). A close-up view of the FtsZ toroid suggests a partially ordered arrangement of filaments in the toroidal structure (Fig. 2c).

Quantitative analysis of the toroidal structure showed a conserved organization, with an outer diameter in the range of the bacterial cell size (502 ± 55 nm) (Fig. 2d), a typical thickness of 127 ± 25 nm (Fig. 2e) and an average height of 93 ± 15 nm (Supplementary Fig. 5b). By measuring the shortest and longest axes, we determined that the circularity of the structure was 0.92 ± 0.1 and 0.85 ± 0.1 for the outer and inner diameter, respectively (Supplementary Fig. 5c). This conserved toroidal structure could arise from the intrinsic curvature of the FtsZ filaments stabilized by ZapD connections.

FtsZ bundle formation increases at higher concentrations of ZapD, showing a strong dependence on protein ratios (Supplementary Fig. 5a). At sub-equimolar concentrations, we could not observe FtsZ bundles, in agreement with previous studies[45,75,78] and light scattering experiments (Fig. 1b, Supplementary Fig. 3). At molar ratios of 1:1 or 1:2 (FtsZ:ZapD), curved bundles and toroidal structures are abundant (Supplementary Fig. 5a), with some single and double FtsZ filaments (Supplementary Fig. 6). At even higher concentrations of ZapD (typically of 1:4 or 1:6 (FtsZ:ZapD)), we observed the formation of straight bundles with striated patterns between the FtsZ filaments (Supplementary Fig. 6), as well as the presence of some toroidal structures (Supplementary Figs. 5a and 6). Here, the high concentration of ZapD molecules may have increased the number of connections between filaments and ultimately promoted the formation of straight bundles. This indicates that the assembly of FtsZ-ZapD structures is a dynamic process that highly depends on the amount of connections established between filaments. Toroids and curved bundles always coexist, but the ratio shifts from toroids to straight bundles at high ZapD concentrations.

Our data demonstrate that ZapD dimers can crosslink adjacent FtsZ filaments, which self-assemble into bundles and toroidal structures. These toroids are remarkably regular in size that matches the bacterial diameter[16,79,81,83]. This indicates that the inherent curvature of the FtsZ filaments is preserved within a range of ZapD connections[68].

The 3D structure of ZapD-mediated FtsZ toroids revealed by cryo-electron tomography

Visualization of FtsZ toroidal structures using cryo-EM suggested a regular arrangement of the FtsZ filaments within the toroid (Fig. 2c). We then used cryo-electron tomography (cryo-ET) to reveal their three-dimensional (3D) organization with greater precision. We first analyzed ZapD-mediated toroidal FtsZ structures at equimolar concentrations (Supplementary Fig. 7a).

Cryo-ET revealed the dense packing of the toroidal structures, with numerous densities connecting the filaments (Fig. 3a, Supplementary Figs. 7a and 8a). Zoomed-in views of the toroids showed a near parallel alignment of FtsZ filaments (Fig. 3b and Supplementary Fig. 8a). In addition, cross-sectional views of the toroids revealed an elongation of the filaments along the Z direction: FtsZ form rather small vertical sheets than filaments. A small elongation in Z is expected due to the missing wedge artefacts in cryo-ET; however, the observed elongation goes far beyond this effect and reveals an intrinsic property of FtsZ structures. FtsZ minisheets are either aligned or shifted in Z, while remaining fairly parallel to each other, with lateral connections between them (Fig. 3c left and Supplementary Fig. 8d).

We then extracted the isosurface of the toroids from the tomograms (Fig. 3c right, 3d, Supplementary Fig. 8b and Supplementary movie 1). This allowed us to visualize the 3D structure of the toroids (Fig 3e, Supplementary Fig. 8c, e and Supplementary Movie 1), consisting of parallel FtsZ minisheets connected by lateral connections, presumably mediated by ZapD (Fig 3e and Supplementary Fig. 8c and e).

To assess the role of ZapD in the formation of the observed lateral connections, we compared the isosurfaces of single and double filaments in the absence of ZapD (Supplementary Fig. 9a) with the individual filaments extracted from the toroids (Supplementary Fig. 9b). FtsZ filaments were similar regardless of the presence of ZapD. However, filaments extracted from toroids were decorated by additional densities (Supplementary. Fig. 9b), which were not found in the absence of ZapD, suggesting that they correspond to ZapD proteins interacting with FtsZ filaments, as observed within the toroidal structure (Fig. 3e and Supplementary Fig. 8c and e).

ZapD plasticity is essential for toroid shape and stabilization

Next, we identified putative ZapD connections within the toroids (Fig. 4a; Supplementary Movie 2). Most connections showed a characteristic bi-spherical shape connecting filaments, reminiscent of ZapD dimers (Fig. 4 b-d). A large variability in the putative ZapD connections gives rise to the overall toroidal structure. We found lateral connections between two parallel FtsZ filaments (or minisheets) at the same toroid height (Fig 4. b). FtsZ filaments at different heights can connect diagonally through ZapD connections, forming a 3D mesh (Fig. 4c, d and Supplementary Movie 2). We also identified the presence of putative ZapD proteins decorating a single FtsZ filament, which can be used to connect other nearby filaments (Fig. 4b). In addition, more than one connection between two filaments occurs, allowing strong attachment between the filaments (Fig. 4d).

Visualization of the 3D filament organization showed that the toroid is formed by a discontinuous arrangement of short, laterally connected filaments (Supplementary Fig. 10a), forming a dense 3D mesh (Fig 4.a and supplementary Fig. 8e). Filament discontinuity does not correlate with a higher number of ZapD connections (Supplementary Fig. 10b), indicating that ZapD is able to crosslink filaments without causing filament breakage. ZapD can crosslink individual filaments laterally in all spatial orientations, resulting in a 3D toroidal structure of

curved filaments parallel to each other and connected across the height of the toroid. Therefore, the preferential curvature of the filaments is conserved by the lateral connections through ZapD at equimolar concentrations, essential for the formation of regular and bacterial-sized toroids[68].

3D imaging of ZapD-mediated FtsZ toroidal structures by cryo-ET provided crucial information about the 3D organization, connectivity and length of filaments inside the toroid. Our data revealed that toroids consist of a discontinuous arrangement of FtsZ filaments connected by ZapD dimers, resulting in a conserved toroidal structure that has never been observed before following the interaction between FtsZ and one of its natural partners *in vitro*.

A high density of ZapD connections promotes the formation of straight FtsZ bundles

Our cryo-ET results showed that ZapD dimers crosslink FtsZ filaments and establish multiple connections between the filaments in toroids, thereby enhancing their interaction (Fig. 4). Biochemical analyses as well as cryo-EM experiments indicate an important role of the FtsZ:ZapD ratio in the formation of toroidal structures or straight bundles (Supplementary Fig. 5a and Supplementary Fig. 6). We then explored how higher densities of ZapD lead to the formation of straight bundles using cryo-ET.

Using the same approach as for the toroids, we collected tomograms of the straight bundles and extracted their isosurfaces (Fig. 5a, Supplementary Fig. 7b and Supplementary Movie 3). The straight bundles are formed at high ZapD concentrations and consist of a highly organized stack of well aligned FtsZ filaments (Fig. 5b). Filaments are connected by multiple ZapD proteins, which straighten the structure of the inherently curved filament (Fig. 5c). Interestingly, ZapD does not crosslink FtsZ filaments laterally but from the top or the bottom of the filaments forming a row of ZapD proteins interacting with both filaments (Fig. 5d). The distance between ZapD proteins provided a mean value of 4.5 ± 0.5 nm (Supplementary Fig. 11b), which is consistent with the size of FtsZ[24]. This suggests that all FtsZ proteins interact with the ZapD dimers that crosslink the filaments. On the other hand, the distance between two FtsZ filaments connected by multiple ZapD proteins was found to be larger than in the absence of ZapD (from 5.9 ± 0.8 nm to 7.6 ± 1.5 nm) (Supplementary Fig.11a). This indicates that ZapD not only connects FtsZ filaments laterally but also stretches them, which could have important implications for the functionality of the FtsZ ring.

These results reveal the important role of the FtsZ:ZapD ratio and the number of connections between filaments in the crosslinking mechanism (Fig. 6). Saturating FtsZ filaments with ZapD proteins straighten their structure and arranges them into large straight bundles. This supports that an equimolar ratio of FtsZ and ZapD is optimal to maintain the preferential curvature of the FtsZ filaments and allow toroid assembly.

Dimerization of ZapD is essential to form FtsZ toroids

Our results suggest that ZapD dimers connect two FtsZ filaments, although the role of dimerization has not yet been experimentally established[74]. We therefore investigated whether the dimerization of ZapD was essential to assemble straight bundles and toroidal structures. To test this, we produced a mutant of ZapD ("mZapD") by substituting three amino acids (R20, R116 and H140) involved in its dimerization by Alanine, thus decreasing the stability of the dimerization interface (Supplementary Fig. 12a).

mZapD can interact with unpolymerized FtsZ-GDP as evidenced by fluorescence anisotropy and FCS (Supplementary Fig. 12b and c). mZapD is still able to promote FtsZ bundle formation but to a much lower extent than wild-type ZapD, as shown by light scattering (Supplementary Fig. 12d). We also visualized these bundles by cryo-EM and observed the formation of thinner bundles (Supplementary Fig. 13b and c). However, toroidal structures and straight bundles were absent in these samples even at high concentrations of mZapD (1:6 molar ratios of FtsZ and mZapD). This indicates that a stable dimerization interface is required to assemble ZapD-mediated structures (Supplementary Fig 13a).

These results demonstrated that dimerization of ZapD is essential to promote the assembly of toroidal structures and straight bundles, although it is not required to promote filament bundling.

Discussion

In this study, we demonstrate that ZapD proteins laterally crosslink FtsZ filaments, forming discontinuous multilayered toroidal structures of the bacterial size. Exploration of these structures using cryo-ET revealed their 3D organization, providing essential information on the molecular mechanism behind filament crosslinking into organized macrostructures. We also highlighted the importance of FtsZ:ZapD protein ratios and ZapD dimerization for FtsZ toroid assembly. This work expanded the current understanding of the FtsZ-ZapD interaction, providing new insights into the crosslinking of FtsZ filaments and the structure of a functional Z ring.

Specifically, we show the assembly of FtsZ filaments into toroidal structures by lateral crosslinking through ZapD. Preferential assembly of toroids in solution likely is a physiologically relevant process given their similarities in shape and size to the Z ring in the cell[16,63,79,80,84,85]. Furthermore, these toroidal structures are an excellent example of what Erickson and coworkers have termed the "intermediate curved conformation" of FtsZ filaments, which appears to be widespread, as evidenced by many studies performed in vitro and in vivo (see Erickson and Osawa 2017[68] for more details). In qualitative agreement with our observations, single-stranded FtsZ filaments can form ring-like structures with a 100-200 nm diameter, as revealed by negative stain EM and AFM[20,23–25,32,86–88]. FtsZ can also form lateral interactions among filaments in response to environmental conditions and assemble into macrostructures[30,46,58,60,65]. Surprisingly, using negative stain TEM, Popp and coworkers also observed the formation of toroidal structures under non-physiological additives such as methylcellulose and polyvinyl alcohol (PVA)[37]. The size of these toroids range from 100 – 500 nm diameter, similar to what we observed here (Fig. 2d and e). However, unlike the toroidal structures formed in the presence of ZapD, no evidence of disassembly upon GTP consumption has been described.

The formation of toroidal structures as a result of filament crosslinking in solution is a clear evidence of the robust preferential curvature of the FtsZ filaments favored by nature to form bacterial-sized ring-like structures[16,68]. The presence of ZapD can help, shape and provide stability to the network, spacing the filaments and crosslinking them into a discontinuous toroid. These features can be further modulated by surface effects at the cell membrane, acting as a scaffold for protein self-organization, a process analyzed experimentally[67,89–93]. In addition, FtsZ can also polymerize into ~1µm diameter ring-like vortices when bound to artificial membranes, either through ZipA[94], FtsA[95], or using a membrane-targeting variant of FtsZ[96].

Interestingly, ZapA proteins can crosslink FtsZ filaments into bundles on the membrane without affecting their treadmilling dynamics[97]. This suggests that lateral interactions through Zap proteins can promote bundling without affecting significantly filament dynamics, consistent with their role inside the cell.

We also demonstrated that ZapD-mediated FtsZ toroids recapitulate many of the structural features of the FtsZ ring architecture *in vivo.* The current model of the Z ring based on super-resolution imaging and cryo-ET, defines a somewhat discontinuous and heterogeneous structure composed of randomly overlapping filaments[63,79,84]. They are arranged in a belt-like macromolecular entity containing nodes with a higher density of dispersed filaments, with the FtsZ filaments confined to a toroidal zone of about 80–100 nm width and approximately 40–60 nm radial thickness, located 13-16 nm below the inner membrane[63,69,79,81,84,85,98,99]. These dimensions are similar to the ones of the toroidal structures promoted by ZapD (Fig. 2d and e, Supplementary Fig. 5b).

The Z ring model also suggests that FtsZ filaments are weakly associated with each other via protein factors such as Zaps and weak FtsZ-FtsZ interactions, which may play a crucial role in their functionality[4,16,59,60,102]. The similarities of the Z ring to the toroidal structures support the important role of FtsZ-associated proteins for filament crosslinking and the mechanism behind Z ring assembly. Structural characterization of the toroids using cryo-ET identified individual ZapD dimers crosslinking the filaments (Fig. 4). We also confirmed a large variability in the conformation of the connections between filaments. Because ZapD is a dimeric protein, it might be expected to act as a rigid linker; however, interaction with FtsZ via the central hub could provide additional spatial freedom to connect other filaments in various conformations, enabling different filament organizations and heterogenicity in the structure (Fig. 4 b-d). This suggests that these crosslinkers act as modulators within the ring structure, spacing the filaments and allowing them to slide[61,63,66,89,93]. The ability of FtsZ to treadmill directionally[95,96,103–105], together with a discontinuous antiparallel organization of transiently crosslinked filaments, is hypothesized to underlie the functionality of the Z ring and force constriction[65–68,106–108]. Thus, Zap proteins can ensure correct filament placement and stabilization, which is consistent with the toroidal structure assembled by ZapD.

We found a significant dependence of ZapD concentration in the crosslinking and assembly of FtsZ macrostructures. Saturation of ZapD proteins connecting FtsZ filaments promoted their assembly into straight bundles, which was never observed at lower ZapD concentrations (Fig. 5 and Supplementary Fig. 7b). This organization results from increased ZapD connections between FtsZ filaments (Fig. 5b-d). The presence of multiple lateral interactions between filaments can reduce the flexibility required to form the toroidal structure, forcing the filaments into a straight bundle conformation. Therefore, we can hypothesize that the assembly of functional FtsZ macrostructures occurs only within a specific range of lateral interactions. At the same time, an increase in these lateral connections would shift the interaction toward the assembly of non-functional, probably rigid and less dynamic straight bundles (Fig. 6). This, along with the large conformational variability found in ZapD connections, may indicate that ZapD can modulate the behavior of the entire structure based on a concentration-dependent mechanism and due to its high plasticity.

The assembly of FtsZ macrostructures promoted by ZapD may also open new horizons for the biochemical reconstitution of contractile division engines in cell-like test tubes[109–111] in the framework of bottom-up synthetic biology[112,113]. Our preliminary results show that crosslinking of filaments by ZapD promoted the formation of dynamic FtsZ bundles within lipid vesicles that disassembled over time (Supplementary Fig. 13 and 14).

To summarize, we demonstrate the assembly of FtsZ toroidal structures formed by a discontinuous arrangement of filaments stabilized by crosslinking with ZapD dimers, which are consistent with some of the structural features of the FtsZ ring observed *in vivo.* We also proposed a concentration-dependent molecular mechanism of filament crosslinking based on previous studies of the interaction and new insights gained from our results. Our in vitro study provides new information on the organization and stabilization of FtsZ filaments in a ring-like structure that can improve our understanding of the Z ring stabilization and thus the entire division process.

Methods

Protein purification: ZapD protein has been overproduced and purified following the procedure previously described in[45] with some modifications. The bacterial strain was an *E. coli* BL21 (DE3) transformed with pET28b-h10-smt3-ZapD fusion plasmid[45]. The cells were sonicated for 6-8 cycles of 20 secs and centrifuged at 40.000 rpm in MLA 80 rotor (Beckman coulter) for 45 min. The protein was eluted by chromatography in 5-ml HisTrap (GE Healthcare) and digested with Smt3-specific protease Ulp1 (SUMO protease encoded in Rosetta pTB145), at 1:1 molar relation. Digestion proceeded for two dialysis of 1 hour at 4°C to avoid protein precipitation. ZapD and His-Smt3 were separated by chromatography in 5-ml HisTrap (GE Healthcare), then the protein was eluted in a 5-ml HiTrap Desalting column (Healtcare) to eliminate completely possible traces of free phosphates in the buffer. Final concentration of ZapD was determined by absorbance at 280 nm using an extinction coefficient (ε) of 25230 M^{-1} cm^{-1} and ZapD purity was checked by SDS-polyacrylamide gel electrophoresis. Protein fractions were frozen in buffer 50 mM KCL, 50 mM Tris-CL, 10 mM $MgCl_2$, 0.2 mM DTT and 2% glycerol. ZapD mutant (mZapD) was purified following the same procedure using the corresponding plasmid. *E. coli* FtsZ was overproduced and purified following the calcium precipitation method described previously[82]. Briefly, E. coli BL21 (DE3) pLysS cells were transformed with pET11b-FtsZ, grown in LB medium and selected with Ampicillin 100 µg/mL. After induction and growth, the pellet was resuspended in PEM buffer (50 mM PIPES-NaOH, pH 6.5, 5 mM $MgCl_2$, 1 mM EDTA) and disrupted using a tip sonicator for 3-4 cycles. The lysate was then separated by centrifugation for 30 min at 20,000 x g at 4 °C, and the supernatant was mixed with 1 mM GTP, 20 mM $CaCl_2$ and incubated at 30 ºC for 15 min to induce FtsZ polymerization and bundling. Subsequently, the FtsZ bundles were pelleted by centrifugation for 15 min at 20,000 x g at 4 °C, and the pellet was resuspended in PEM buffer and centrifuged again for 15 min at 20,000 x g, 4 °C, collecting the supernatant. Precipitation and resuspension steps were repeated to improve the purification. The buffer was then exchanged using an Amicon Ultra-0.5 centrifugal filter unit 50 kDa (Merck KGaA). FtsZ purity was checked by SDS-polyacrylamide gel electrophoresis and concentration was determined by absorbance at 280 nm using an extinction coefficient (ε) of 14000 M^{-1} cm^{-1} [82]. Protein solutions were aliquoted, frozen in liquid nitrogen, and stored at -80 °C until further use.

Plasmid Design and Molecular Cloning: To generate the ZapD mutant (mZapD), seamless cloning method was used according to the provider's protocol (ThermoFisher Scientific /Invitrogen GeneArt™ Seamless Cloning and Assembly Enzyme Mix (A14606)) using the plasmid pET28b-h10-smt3-ZapD and the primers listed in (Supplementary Table 1). All enzymes for cloning were from Thermo Fisher Scientific (Waltham, MA, USA). Briefly, DNA fragments were amplified with Phusion High-Fidelity DNA Polymerase andorigo primers (Sigma–Aldrich, St. Louis, MO, USA). Then, PCR products were treated with DpnI and

combined using GeneArt Seamless Cloning and Assembly Enzyme Mix. The plasmid was propagated in E. coli OneShot TOP10 (Thermo Fisher Scientific) and purified using NucleoBond Xtra Midi kit (Macherey-Nagel GmbH, Duren, Germany). Directed site mutagenesis was made by substituting three amino acids in the ZapD sequence by Alanine (R20, R116, H140). The plasmid was then verified using Sanger Sequencing Service (Microsynth AG, Balgach, Switzerland).

Protein labelling: Covalent labelling of FtsZ with Alexa 488 the amino groups of N-terminal amino acid residue with Alexa Fluor 488 carboxylic acid succinimidyl ester dye following the procedure previously described[22]. ZapD and mZapD were labelled with ATTO-647N carboxylic acid succinimidyl ester dye in the amino group. Before the reaction, ZapD was dialyzed in 20 mM HEPES, 50 mM KCl, 5 mM $MgCl_2$, pH 7.5 and the probe was dissolved in Dimethylsulfoxide (DMSO). The reaction was allowed to proceed for 35-60 min at RT and stopped with 10 % Tris-HCl 1 M. The free dye was separated from labelled protein by a Hi-TRAP Desalting column (GE Healthcare). The final degree of labelling of FtsZ and ZapD was calculated from the molar absorption coefficients of the protein and the dye. It was around 0.5 moles of probe per mole of FtsZ and around 0.3/0.4 moles of dye per mole of ZapD.

Analytical ultracentrifugation; sedimentation velocity (SV) and sedimentation equilibrium (SE): Sedimentation velocity assays were performed to detect the homogeneity and association state of individual proteins and the stoichiometry of the formed protein-protein complexes. In brief, the experiments were carried out at 43-48 Krpm in an Optima XL-I analytical ultracentrifuge, equipped with UV–VIS absorbance and Raleigh interference detection systems. The sedimentation coefficient distributions were calculated by least-squares boundary modeling of sedimentation velocity data using the c(s) method[114] as implemented in the SEDFIT program. The s-values of the present species were corrected to standard conditions (pure water at 20ºC, and extrapolated to infinite dilution) to obtain the corresponding standard s-values (s20,w) using the program SEDNTERP[115]. Multi-signal sedimentation velocity (MSSV) data were globally analyzed by SEDPHAT software[116] using the “multi-wavelength discrete/continuous distribution analysis” model, to determine the spectral and diffusion deconvoluted sedimentation coefficient distributions, ck(s), from which the stoichiometry of protein complexes can be derived[117]. Sedimentation equilibrium of ZapD was carried out to confirm the association state of the protein in the same experimental conditions and concentration range tested by sedimentation velocity (2-30 µM). Short columns (100 µL) SE experiments were carried out at 14000 and 10000 rpm. Weight-average buoyant molecular weights were obtained by fitting a single-species model to the experimental data using the HeteroAnalysis program[118], once corrected for temperature and buffer composition with the program SEDNTERP[115].

Light scattering assay: Light scattering of protein samples was collected by measuring the absorbance at 350 nm in a TECAN plate reader (Tecan Group Ltd., Mannedorf, Switzerland). All samples reached a final volume of 50 µL in a 364-Well Flat-Bottom Microplate (UV-Star, Greiner Bio-One GmbH) before measuring the absorbance. Different concentrations of FtsZ and ZapD were premixed in the well-plate and measured before addition of GTP to extract subsequently the individual blank values. Concentrations of FtsZ and ZapD varied from 0 to 80 µM and buffer conditions are specified in each graph and the caption of the figures ranging from 50 to 500 mM KCl, 6 to 8 pH, always supplemented with 50 mM Tris-Cl and 5 mM $MgCl_2$. Manual mixing was performed after addition of GTP and orbital oscillations for 5 sec in the TECAN were made prior to any measurement to avoid sedimentation of the samples. Time

measurements were taken as specified in each condition. Reported values are the average of 3-12 independent measurements ± Standard deviation.

GTPase activity of FtsZ: GTPase activity of FtsZ was measured by quantification of the inorganic phosphate with a colorimetric assay (BIOMOL GREENÒ kit from ENZO life sciences) for two minutes. 5 µM FtsZ was used in our standard buffer (5 mM $MgCl_2$, 50 mM Tris-HCl, 50 mM KCl, pH 7) or buffers at higher KCl concentrations (50-500 mM KCl) and polymerization was triggered by 1 mM GTP. ZapD was added at different concentrations and premixed with FtsZ before addition of GTP. 13 µL fractions were added to a 96-Well Flat-Bottom Microplate (UV-Star, Greiner Bio-One GmbH) every 20 sec after addition of GTP and mixed with the Reaction buffer reaching 50 µL and 100 µL of BIOMOL GREEN reagent, to stop the reaction. After stopping the reaction, samples were incubated for 10 min at RT and the absorbance was measured at 620 nm in a Varioskan Flash plate reader (Thermo Fisher Scientific, MA, USA). Concentrations of inorganic Phosphate were calculated from a phosphate standard curve, while the GTPase activity reaction rate (V, mol P/mol FtsZ/ min) was determined from the slope of the linear part of phosphate accumulation curves.

Preparation of EM grids. Cryo-EM grids were plunge frozen with a Vitrobot Mk.IV (Thermo Fischer Scientific) using 3 µL of the samples applied to previously glow discharged R 2/1 Holey Carbon Cu 200 mesh EM grids (Quantifoil). Samples were 10 µM FtsZ with or without ZapD or mZapD at different concentrations specified in each case (0 – 60 µM). Proteins were mixed in our working buffer containing 50 mM, 5 mM $MgCl_2$, 50 mM Tris-HCl, pH 7. Samples were incubated for 2 minutes after the addition of 1 mM GTP to trigger polymerization. The Vitrobot was set to 4° C, 100% humidity, blot time 3 s, blot force 3. Whatman no. 1 filter paper was used for blotting and liquid ethane kept at liquid nitrogen temperatures was used as a cryogen for vitrification.

Cryo-EM and cryo-ET. Cryo-EM data was acquired on two microscopes as follows. Cryo-EM micrographs were acquired within SerialEM[119] on a Talos Arctica transmission electron microscope (Thermo Fisher Scientific) operated at 200 kV, equipped with a Falcon III (Thermo Fisher Scientific) direct electron detector operated in integrating mode. Images were recorded at 73,000x magnification (pixel size 1.997 Å) and 92,000x magnification (pixel size 1.612 Å) at -2.5 µm to -5 µm target defocus with an approximate total electron dose of 60 electrons / $Å^2$.

Cryo-EM micrographs and Cryo-ET tilt series were acquired within SerialEM on a G2 Titan Krios transmission electron microscope (Thermo Fisher Scientific) operated at 300 kV, equipped with a FEG, post-column energy filter (Gatan) and a K3 camera (Gatan) operated in electron counting mode. Micrographs were recorded at 42,000x magnification (pixel size 2.154 Å) at -5 µm target defocus with an approximate total electron dose of 60 electrons / $Å^2$. Tilt series were recorded at 42,000x magnification (pixel size 2.154 Å) at -5 µm target defocus with an approximate total electron dose of 100-140 electrons / $Å^2$. Acquisition was performed using a dose-symmetric tilt scheme, a tilt range of +/-60°, an angular increment of 2°.

Tomogram reconstruction: Tilt series preprocessing was performed using the TOMOMAN package (https://github.com/williamnwan/TOMOMAN). In brief, MotionCor2[120] was used to align individual frames, followed by cumulative dose-weighting using an exposure-dependent attenuation function, as described in[121]. Dose-weighted tilt series were aligned using IMOD[122] either by employing gold fiducials (if available) or by patch-tracking, and binned tomograms (pixel size 8.616 Å) were generated using weighted back-projection. Stacks were split into odd

and even frames to generate half-set tomograms which were used for training and subsequent denoising in cryoCARE[123].

Denoised tomograms were directly employed for segmentation of the toroids, straight bundles and individual filaments by cropping an area of interest and displaying the volume as isosurface in USCF ChimeraX[124]. To highlight connections between filaments, the respective parts were cropped from the volume using the Volume Eraser tool in USCF Chimera[125].

All micrographs and slices through tomograms were visualized using IMOD. Isosurface renderings of toroids, straight bundles and individual filaments were displayed using USCF ChimeraX and USCF Chimera.

Fluorescence anisotropy: Anisotropy measurements were performed using a TECAN plate reader (Tecan Group Ltd., Mannedorf, Switzerland). Excitation and emission wavelengths were 625 nm and 680 nm, respectively. ZapD or mZapD labelled with ATTO 647N were used as fluorescence tracer with a final concentration of 150 nM of ATTO-647N and supplemented with unlabeled ZapD reaching a concentration of 5 µM. FtsZ was added at increasing concentrations to analyze their interaction. Binding affinities (apparent K_D) were determined by fitting the Hill equation to the normalized anisotropy data. Each condition was measured in three independent samples.

Fluorescence correlation spectroscopy (FCS): FCS measurements were performed using a PicoQuant MicroTime200 system equipped with an Olympus 60x, NA1.2 UPlanApo water immersion objective. A pulsed 636 nm diode laser was used to excite fluorescence of Atto647N-labelled ZapD, mZapD or free Atto647N carboxylate (for calibration). Three measurements of 60 s each were performed per sample at room temperature (21°C), and three samples per condition were measured. The repetition rate of the pulsed laser was 26.7 MHz, and the average power was 1 µW at the objective back pupil. Fluorescence was collected through the same objective, spatially filtered through a 50 µm diameter pinhole, and spectrally filtered through a 690/70 nm bandpass filter before being split by a neutral beam splitter onto two avalanche photodiodes (Excelitas SPCM-AQRH-14-TR). Photon count events were digitized using a PicoQuant TimeHarp 260 Nano TCSPC card. Time-correlated single photon counting information was used for monitoring data quality during measurements, but not in further analysis. As especially in samples with FtsZ ZapD, and GTP present simultaneously we occasionally saw large, bright particles that are difficult to treat in FCS analysis, data was subjected to a burst removal algorithm similar to Margineanu et al. [126] and only “non-burst” data was used in correlation analysis to obtain statistics representative of the large number of small oligomer particles, ignoring rare large ones. Cross-correlation functions of the two detectors were calculated and fitted with a standard model for three-dimensional diffusion in with rapid dye blinking:

$$G(\tau) = G_0 \left[\frac{1 - F_B + F_B e^{-\frac{\tau}{\tau_B}}}{1 - F_B} \right] \frac{1}{1 + \frac{\tau}{\tau_d}} \sqrt{\frac{1}{1 + \frac{\tau}{S^2 \tau_d}}}$$

With amplitude G_0, diffusion time τ_d, point spread function aspect ratio S, and blinking parameters F_B and τ_B. Custom software was written in Python for burst removal, correlation, and fitting, based on tttrlib 0.0.19 (https://github.com/Fluorescence-Tools/tttrlib). The software is in ongoing development, and available upon request.

Fluorescence Microscopy: Images of lipid vesicles were recorded on a Zeiss LSM780 confocal laser scanning microscope using a Zeiss C-Apochromat x40/1.20 water-immersion objective (Carl Zeiss AG, Oberkochen, Germany). FtsZ-Alexa 488 was excited using a 488 nm argon laser, while ZapD-ATTO 647N and DOPE-ATTO 655 were excited by the 633 nm HeNe laser. All confocal images were processed using ImageJ.

Fluorescence recovery after photobleaching (FRAP): On lipid vesicles, a circular spot on the bundle was illuminated with full 488 laser power for 0.164 s (10 iterations on the Zen Black software (Carl Zeiss AG, Oberkochen, Germany)). The average fluorescence intensity was recorded every 5 second for 250 seconds and the mean intensity in a second area of the same dimensions was recorded in the same field of view to correct for the intensity drift. The fluorescence intensity was then corrected and normalized to facilitate its interpretation. The data represents 5 independent measurements and the standard deviation from different vesicles in 3 different samples.

Preparation of lipid vesicles: Lipid vesicles were prepared following the double emulsion principle[109,127].1-palmitoyl-2-oleoyl-glycero-3-phosphocholine (POPC) and 1-palmitoyl-2-oleoyl-sn-glycero-3-phospho-(1'-rac-glycerol) (POPG) (Avanti Polar Lipids, Alabaster, AL, USA) were mixed and dissolved in chloroform at 25 g/L in a molecular ratio of 7:3. 100 µL of the lipid mixture was dried by nitrogen gas stream and 10 µL of decane (TCI Deutschland GmbH, Eschborn, Germany) was added to resuspend the lipids inside a N_2 globe box at low humidity. Subsequently, 1 mL of mineral oil (Carl Roth GmbH, Karlsruhe, Germany) was added and vortexed for 1 min to prepare a lipid-oil mixture. To form the lipid vesicles, a 96-well Flat-Bottom Microplate (SensoPlate, Greiner Bio-One GmbH, Kremsmuenster, Austria) was used for both, vesicle formation and visualization. The inner and outer solutions were prepared in working buffer at the same osmolarity, which was measured using an osmometer (Fiske Micro-Osmometer model120, Fiske Associates, Norwood, MA, USA). Sucrose and glucose 100 mM were added in outer and inner solutions respectively to create a density gradient. 100 µL of the outer solution was added into a well in a 96 well-plate, and subsequently, 50 µL of the lipid-oil mixture was layered on top of the outer solution. Emulsion solution containing the protein mixture was obtained from 2 µL of the inner solution and 100 µL of the lipid-oil mixture mixed in a 1.5 mL tube by tapping. Then, ~80 µL of this emulsion solution was dripped on the multi-layered solution. Next, lipid vesicles were obtained by centrifugation for 10 min at 1500 rcf at room temperature and directly visualized under the confocal microscope. FtsZ (5 µM) and ZapD (0 - 20 µM) were added at different protein ratios and 1 mM GTP was added to trigger FtsZ polymerization in working buffer. To allow visualization of the membrane in confocal microscopy, 0.01% Mol of DOPE-ATTO 655 was added to the lipid mixture.

Image analysis: Electron microscopy images were processed and analyzed using IMOD and ImageJ. The dimensions of the toroidal structures, FtsZ bundles and distances between filaments were manually measured using ImageJ and IMOD. Distances were plotted as histograms using Origin (OriginPro, Version *2019b*. OriginLab Corporation, Northampton, MA, USA.). For each toroid analyzed (n = 67) the inner and outer diameter were measured collecting the major and minor distance in each case. The circularity of the toroid was the result of the division between the minor diameter divided by major diameter for each toroid. The height of the FtsZ toroid was manually measured from the tomograms, collecting 4 measurements per toroid to assure a correct representation of the size (n = 17). For the distances between double filaments and straight bundles, they were also manually measured by using IMOD. Each measurement represents only one FtsZ double filament or one FtsZ-

ZapD double filament, however, the same bundle could be measured more than once as they are composed for multiple filaments. The measurements were collected from >3 independent samples. The distances between ZapDs connecting two FtsZ filaments were measured following the same methodology. The mean value and standard deviation of different datasets were calculated and added to the figures together with the n used for each case.

Acknowledgements

We thank Daniel Bollschweiller (MPIB cryo-EM facility) and Rafael Nuñez (CIB-CSIC imaging facility) for their help with the cryo-EM experiments. We also thank the MPIB core facility for assistance in protein purification, Michaela Schaper for plasmid cloning, Sigrid Bauer for lipid preparation and Noelia Ropero, Katharina Nakel and Kerstin Andersson for protein purification. We are also grateful to Miguel Robles-Ramos, Ana Raso, Hiromune Eto, Cristina Capitanio, Pedro Weickert, Kareem Al-Nahas, Yusuf Qutbuddin, Silvia Zorrilla, Henri Franquelim, Diego Ramirez and Daniela Garcia-Soriano for helpful discussions and fruitful input in this work. This project has been supported by the Max Planck-Bristol Centre for Minimal Biology (A.M.-S.) and the Deutsche Forschungsgemeinschaft (P. S.). J.S. and M. Jasnin are supported by the French Agence Nationale de la Recherche (ANR) and the Deutsche Forschungsgemeinschaft (DFG) call ANR-DFG 2020 NLE for the project no. JA-3038/2-1 (to M. Jasnin). J.-H.K. is funded by the Germany´s Excellence Strategy – EXC-2094 – 390783311. This work was also supported by the Spanish Government through Grant PID2019-104544GB-I00/AEI/10.13039/501100011033 (M.Jimenez, C.A. and G.R.). M.S.-S. was supported by European Social Fund through Grant PTA2020-018219-I/AEI/10.13039/501100011033. J.R.L.-O and M S.-S. acknowledge support from the Molecular Interactions Facility at the CIB Margarita Salas-CSIC. A.M.-S and J.-H.K. are part of IMPRS-LS, J.-H.K. is also a CeNS Center for NanoScience associate.

Author contributions

A.M.-S., M. Jiménez and G.R. conceived the study. A.M.-S. purified and fluorescently labelled ZapD and FtsZ. M.S.-S. performed FtsZ GTPase assays. A.M.-S. and J.-H.K. designed, performed and analyzed FCS and fluorescence anisotropy experiments. A.M.-S. and M. Jiménez designed and performed light scattering assays. M. Jiménez, C.A. and J.R.L.-O. designed, performed and analyzed the AUC data. A.M.-S., J.S., T.S. and M. Jasnin designed, performed, and analyzed the cryo-EM and cryo-ET experiments. L.B. designed the plasmid and purified mZapD. A.M.-S. performed the encapsulation in lipid vesicles. A.M.-S. wrote the original draft. A.M.-S., L.B., M. Jiménez, M. Jasnin, G.R. and P.S. revised the manuscript and figures. All authors discussed the results and revised the manuscript

References

1. Levin, P. A. & Janakiraman, A. *Localization, Assembly, and Activation of the Escherichia coli Cell Division Machinery*. https://journals.asm.org/journal/ecosalplus (2021).

2. den Blaauwen, T., Hamoen, L. W. & Levin, P. A. The divisome at 25: the road ahead. *Curr. Opin. Microbiol.* **36**, 85–94 (2017).

3. Du, S. & Lutkenhaus, J. Assembly and Activation of the *Escherichia coli* Divisome. *Mol. Microbiol.* **105**, 177–187 (2017).

4. Du, S. & Lutkenhaus, J. At the Heart of Bacterial Cytokinesis: The Z Ring. *Trends in Microbiology* (2019) doi:10.1016/j.tim.2019.04.011.

5. Attaibi, M. & Den Blaauwen, T. An Updated Model of the Divisome: Regulation of the Septal Peptidoglycan Synthesis Machinery by the Divisome. (2022) doi:10.3390/ijms23073537.

6. Nogales, E., Downing, K. H., Amos, L. A. & Löwe, J. Tubulin and FtsZ form a distinct family of GTPases. *Nat. Struct. Biol. 1998 56* **5**, 451–458 (1998).

7. Erickson, H. P. FtsZ, a prokaryotic homolog of tubulin? *Cell* **80**, 367–370 (1995).

8. Mukherjee, A., Dai, K. & Lutkenhaus, J. Escherichia coli cell division protein FtsZ is a guanine nucleotide binding protein. *Proc. Natl. Acad. Sci. U. S. A.* **90**, 1053–1057 (1993).

9. De Boer, P., Crossley, R. & Rothfield, L. The essential bacterial cell-division protein FtsZ is a GTPase. *Nat. 1992 3596392* **359**, 254–256 (1992).

10. Escobar-Henriques, M. & Anton, F. Mechanistic perspective of mitochondrial fusion: Tubulation vs. fragmentation. *Biochimica et Biophysica Acta - Molecular Cell Research* (2013) doi:10.1016/j.bbamcr.2012.07.016.

11. RayChaudhuri, D. & Park, J. T. Escherichia coli cell-division gene ftsZ encodes a novel GTP-binding protein. *Nature* **359**, 251–254 (1992).

12. Bramhill, D. & Thompson, C. M. GTP-dependent polymerization of Escherichia coli FtsZ protein to form tubules. *Proc. Natl. Acad. Sci. U. S. A.* **91**, 5813 (1994).

13. Lutkenhaus, J. & Addinall, S. G. Bacterial cell division and the Z ring. *Annu. Rev. Biochem.* **66**, 93–116 (1997).

14. Addinall, S. G., Erfei, B. & Lutkenhaus, J. FtsZ ring formation in fts mutants. *J. Bacteriol.* **178**, 3877–3884 (1996).

15. Wang, M., Chao Fang, ·, Ma, B., Luo, X. & Hou, Z. Regulation of cytokinesis: FtsZ and its accessory proteins. *Curr. Genet.* **66**, 43–49 (2020).

16. Mcquillen, R. & Xiao, J. Insights into the Structure, Function, and Dynamics of the Bacterial Cytokinetic FtsZ-Ring. (2020) doi:10.1146/annurev-biophys-121219.

17. Goehring, N. W., Gonzalez, M. D. & Beckwith, J. Premature targeting of cell division proteins to midcell reveals hierarchies of protein interactions involved in divisome assembly. *Mol. Microbiol.* **61**, 33–45 (2006).

18. Small, E. & Addinall, S. G. Dynamic FtsZ polymerization is sensitive to the GTP to GDP ratio and can be maintained at steady state using a GTP-regeneration system. *Microbiology* **149**, 2235–2242 (2003).

19. Söderström, B., Daniel, · & Daley, O. The bacterial divisome: more than a ring? *Curr Genet* **63**, 161–164 (2017).

20. Erickson, H. P., Taylor, D. W., Taylor, K. A. & Bramhill, D. Bacterial cell division protein FtsZ assembles into protofilament sheets and minirings, structural homologs of tubulin polymers. *Proc. Natl. Acad. Sci. U. S. A.* **93**, 519–523 (1996).

21. Lu, C., Reedy, M. & Erickson, H. P. Straight and curved conformations of FtsZ are regulated by GTP hydrolysis. *J. Bacteriol.* **182**, 164–170 (2000).

22. González, J. M. *et al.* Essential cell division protein FtsZ assembles into one monomer-thick ribbons under conditions resembling the crowded intracellular environment. *J. Biol. Chem.* **278**, 37664–37671 (2003).

23. Mingorance, J. *et al.* Visualization of single Escherichia coli FtsZ filament dynamics with atomic force microscopy. *J. Biol. Chem.* **280**, 20909–20914 (2005).

24. Huecas, S. *et al.* The interactions of cell division protein FtsZ with guanine nucleotides. *J. Biol. Chem.* **282**, 37515–37528 (2007).

25. Hamon, L. *et al.* Mica surface promotes the assembly of cytoskeletal proteins. *Langmuir* **25**, 3331–3335 (2009).

26. Milam, S. L., Osawa, M. & Erickson, H. P. Negative-Stain Electron Microscopy of Inside-Out FtsZ Rings Reconstituted on Artificial Membrane Tubules Show Ribbons of Protofilaments. *Biophys. J.* **103**, 59–68 (2012).

27. Housman, M., Milam, S. L., Moore, D. A., Osawa, M. & Erickson, H. P. FtsZ Protofilament Curvature Is the Opposite of Tubulin Rings. *Biochemistry* **55**, 6 (2016).

28. Romberg, L. & Levin, P. A. Assembly Dynamics of the Bacterial Cell Division Protein FtsZ: Poised at the Edge of Stability. *Annu. Rev. Microbiol.* **57**, 125 (2003).

29. Scheffers, D. J. & Driessen, A. J. M. The polymerization mechanism of the bacterial cell division protein FtsZ. *FEBS Lett.* **506**, 6–10 (2001).

30. Mukherjee, A. & Lutkenhaus, J. Analysis of FtsZ assembly by light scattering and determination of the role of divalent metal cations. *J. Bacteriol.* **181**, 823–832 (1999).

31. Osawa, M., Anderson, D. E. & Erickson, H. P. Supporting Online Material Reconstitution of Contractile FtsZ Rings in Liposomes. *Z. Hu, J. Lutkenhaus, Mol. Microbiol* **52**, 89 (1990).

32. Erickson, H. P. & Stoffler, D. Protofilaments and rings, two conformations of the tubulin family conserved from bacterial FtsZ to alpha/beta and gamma tubulin. *J. Cell Biol.* **135**, 5 (1996).

33. Löwe, J. & Amos, L. A. Tubulin-like protofilaments in Ca2+-induced FtsZ sheets. *EMBO J.* **18**, 2364–2371 (1999).

34. Hale, C. A., Rhee, A. C. & De Boer, P. A. J. ZipA-Induced Bundling of FtsZ Polymers Mediated by an Interaction between C-Terminal Domains. *J. Bacteriol.* **182**, 5153–5166 (2000).

35. Marrington, R., Small, E., Rodger, A., Dafforn, T. R. & Addinall, S. G. FtsZ fiber bundling is triggered by a conformational change in bound GTP. *J. Biol. Chem.* **279**, 48821–48829 (2004).

36. Huecas, S. *et al.* Energetics and Geometry of FtsZ Polymers: Nucleated Self-Assembly of Single Protofilaments. *Biophys. J.* **94**, 1796–1806 (2008).

37. Popp, D., Iwasa, M., Narita, A., Erickson, H. P. & Maéda, Y. FtsZ Condensates: An In Vitro Electron Microscopy Study. (2009) doi:10.1002/bip.21136.

38. Ma, X. & Margolin, W. Genetic and Functional Analyses of the Conserved C-Terminal Core Domain of Escherichia coli FtsZ. *J. Bacteriol.* **181**, 7531–7544 (1999).

39. Pichoff, S. & Lutkenhaus, J. Overview of cell shape: cytoskeletons shape bacterial cells. *Curr. Opin. Microbiol.* **10**, 601–605 (2007).

40. Hale, C. A. & De Boer, P. A. J. Direct Binding of FtsZ to ZipA, an Essential Component of the Septal Ring Structure That Mediates Cell Division in E. coli. *Cell* **88**, 175–185 (1997).

41. Zhan, L., Mukherjee, A. & Lutkenhaus, J. Recruitment of ZipA to the division site by interaction with FtsZ. *Mol. Microbiol.* **31**, 1853–1861 (1999).

42. Mosyak, L. *et al.* The bacterial cell-division protein ZipA and its interaction with an FtsZ fragment revealed by X-ray crystallography. *EMBO J.* **19**, 3179–3191 (2000).

43. Wang, X., Huang, J., Mukherjee, A., Cao, C. & Lutkenhaus, J. Analysis of the interaction of FtsZ with itself, GTP, and FtsA. *J. Bacteriol.* **179**, 5551–5559 (1997).

44. Buss, J. A., Peters, N. T., Xiao, J. & Bernhardt, T. G. ZapA and ZapB form an FtsZ-independent structure at midcell. *Mol. Microbiol.* **104**, 652–663 (2017).

45. Durand-Heredia, J., Rivkin, E., Fan, G., Morales, J. & Janakiraman, A. Identification of ZapD as a cell division factor that promotes the assembly of FtsZ in Escherichia coli. *J. Bacteriol.* **194**, 3189–3198 (2012).

46. Huang, K. H., Durand-Heredia, J. & Janakiraman, A. FtsZ ring stability: Of bundles, tubules, crosslinks, and curves. *J. Bacteriol.* **195**, 1859–1868 (2013).

47. Durand-Heredia, J. M., Yu, H. H., De Carlo, S., Lesser, C. F. & Janakiraman, A. Identification and characterization of ZapC, a stabilizer of the FtsZ ring in Escherichia coli. *J. Bacteriol.* **193**, 1405–1413 (2011).

48. Ebersbach, G., Galli, E., Møller-Jensen, J., Löwe, J. & Gerdes, K. Novel coiled-coil cell division factor ZapB stimulates Z ring assembly and cell division. *Mol. Microbiol.* **68**, 720–735 (2008).

49. Gueiros-Filho, F. J. & Losick, R. A widely conserved bacterial cell division protein that promotes assembly of the tubulin-like protein FtsZ. (2002) doi:10.1101/gad.1014102.

50. Hale, C. A. *et al.* Identification of Escherichia coli ZapC (YcbW) as a component of the division apparatus that binds and bundles FtsZ polymers. *J. Bacteriol.* **193**, 1393–1404 (2011).

51. Woldemeskel, S. A., McQuillen, R., Hessel, A. M., Xiao, J. & Goley, E. D. A conserved coiled-coil protein pair focuses the cytokinetic Z-ring in Caulobacter crescentus. *Mol. Microbiol.* **105**, 721–740 (2017).

52. Raskin, D. M. & de Boer, P. A. J. MinDE-Dependent Pole-to-Pole Oscillation of Division Inhibitor MinC in Escherichia coli. *J. Bacteriol.* (1999) doi:10.1128/jb.181.20.6419-6424.1999.

53. de Boer, P. A. J., Crossley, R. E. & Rothfield, L. I. A division inhibitor and a topological specificity factor coded for by the minicell locus determine proper placement of the division septum in E. coli. *Cell* **56**, 641–649 (1989).

54. Woldringh, C. L., Mulder, E., Huls, P. G. & Vischer, N. Toporegulation of bacterial division according to the nucleoid occlusion model. *Res. Microbiol.* **142**, 309–320 (1991).

55. Tonthat, N. K. *et al.* Molecular mechanism by which the nucleoid occlusion factor, SlmA, keeps cytokinesis in check. *EMBO J.* **30**, 154–164 (2011).

56. Ortiz, C., Natale, P., Cueto, L. & Vicente, M. The keepers of the ring: regulators of FtsZ assembly. *FEMS Microbiol. Rev.* **040**, 57–67 (2016).

57. Buske, P. J., Mittal, A., Pappu, R. V. & Levin, P. A. An intrinsically disordered linker plays a critical role in bacterial cell division. *Semin. Cell Dev. Biol.* **37**, 3–10 (2015).

58. Buske, P. J. & Levin, P. A. Extreme C terminus of bacterial cytoskeletal protein FtsZ plays fundamental role in assembly independent of modulatory proteins. *J. Biol. Chem.* **287**, 10945–10957 (2012).

59. Huecas, S. *et al.* Self-Organization of FtsZ Polymers in Solution Reveals Spacer Role of the Disordered C-Terminal Tail. *Biophys. J.* **113**, 1831–1844 (2017).

60. Sundararajan, K. & Goley, E. D. The intrinsically disordered C-terminal linker of FtsZ regulates protofilament dynamics and superstructure in vitro. *J. Biol. Chem.* **292**, 20509–20527 (2017).

61. Lan, G., Daniels, B. R., Dobrowsky, T. M., Wirtz, D. & Sun, S. X. Condensation of FtsZ filaments can drive bacterial cell division. *Proc. Natl. Acad. Sci. U. S. A.* **106**, 121–126 (2009).

62. Surovtsev, I. V., Morgan, J. J. & Lindahl, P. A. Kinetic Modeling of the Assembly, Dynamic Steady State, and Contraction of the FtsZ Ring in Prokaryotic Cytokinesis. *PLOS Comput. Biol.* **4**, e1000102 (2008).

63. Szwedziak, P., Wang, Q., Bharat, T. A. M., Tsim, M. & Löwe, J. Architecture of the ring formed by the tubulin homologue FtsZ in bacterial cell division. *Elife* **3**, e04601 (2014).

64. Coltharp, C. & Xiao, J. Beyond force generation: Why is a dynamic ring of FtsZ polymers essential for bacterial cytokinesis?; Beyond force generation: Why is a dynamic ring of FtsZ polymers essential for bacterial cytokinesis? doi:10.1002/bies.201600179.

65. Erickson, H. P., Anderson, D. E. & Osawa, M. FtsZ in Bacterial Cytokinesis: Cytoskeleton and Force Generator All in One. *Microbiol. Mol. Biol. Rev.* **74**, 504–528 (2010).

66. Nguyen, L. T., Oikonomou, C. M. & Jensen, G. J. *Simulations of Proposed Mechanisms of FtsZ-Driven Cell Constriction*. https://doi.org/10 (2021).

67. Mateos-Gil, P., Tarazona, P. & ´ Elez, M. V. Bacterial cell division: modeling FtsZ assembly and force generation from single filament experimental data. *FEMS Microbiol. Rev.* **039**, 73–87 (2019).

68. Erickson, H. P. & Osawa, M. FtsZ Constriction Force-Curved Protofilaments Bending Membranes. *Subcell. Biochem.* **84**, (2017).

69. Buss, J. *et al.* In vivo organization of the FtsZ-ring by ZapA and ZapB revealed by quantitative super-resolution microscopy. *Mol. Microbiol.* **89**, 1099–1120 (2013).

70. Schumacher, M. A., Zeng, W., Huang, K. H., Tchorzewski, L. & Janakiraman, A. Structural and functional analyses reveal insights into the molecular properties of the Escherichia coli Z ring stabilizing protein, ZapC. *J. Biol. Chem.* **291**, 2485–2498 (2016).

71. Pazos, M., Natale, P., Margolin, W. & Vicente, M. Interactions among the early Escherichia coli divisome proteins revealed by bimolecular fluorescence complementation. *Environ. Microbiol.* **15**, 3282–3291 (2013).

72. Marteyn, B. S. *et al.* ZapE Is a Novel Cell Division Protein Interacting with FtsZ and Modulating the Z-Ring Dynamics. (2014) doi:10.1128/mBio.00022-14.

73. Bailey, M. W., Bisicchia, P., Warren, B. T., Sherratt, D. J. & Männik, J. Evidence for Divisome Localization Mechanisms Independent of the Min System and SlmA in Escherichia coli. *PLOS Genet.* **10**, e1004504 (2014).

74. Schumacher, M. A., Huang, K. H., Zeng, W. & Janakiraman, A. Structure of the z ring-associated protein, zapd, bound to the c-terminal domain of the tubulin-like protein, ftsz, suggests mechanism of z ring stabilization through ftsz cross-linking. *J. Biol. Chem.* **292**, 3740–3750 (2017).

75. Huang, K. H., Mychack, A., Tchorzewski, L. & Janakiraman, A. Characterization of the FtsZ C-Terminal variable (CTV) Region in Z-Ring assembly and interaction with the Z-Ring stabilizer ZapD in E. coli cytokinesis. *PLoS One* **11**, 1–24 (2016).

76. Choi, H., Min, K., Mikami, B., Yoon, H. & Lee, H. H. Structural and Biochemical Studies Reveal a Putative FtsZ Recognition Site on the Z-ring Stabilizer ZapD. **39**, 814–820 (2016).

77. Son, S. H. & Lee, H. H. Crystallization and preliminary X-ray crystallographic analysis of Z-ring-associated protein (ZapD) from *Escherichia coli*. *Acta Crystallogr. Sect. F Struct. Biol. Commun.* **71**, 194–198 (2015).

78. Roach, E. J. *et al.* Structure and Mutational Analyses of. **198**, 1683–1693 (2016).

79. Fu, G. *et al.* In Vivo Structure of the E. coli FtsZ-ring Revealed by Photoactivated Localization Microscopy (PALM). *PLoS One* **5**, e12680 (2010).

80. Li, Z., Trimble, M. J., Brun, Y. V. & Jensen, G. J. The structure of FtsZ filaments in vivo suggests a force-generating role in cell division. *EMBO J.* **26**, 4694–4708 (2007).

81. Lyu, Z., Coltharp, C., Yang, X. & Xiao, J. Influence of FtsZ GTPase activity and concentration on nanoscale Z-ring structure in vivo revealed by three-dimensional Superresolution imaging. *Biopolymers* **105**, 725–734 (2016).

82. Rivas, G. *et al.* Magnesium-induced linear self-association of the FtsZ bacterial cell division protein monomer. The primary steps for FtsZ assembly. *J. Biol. Chem.* (2000) doi:10.1074/jbc.275.16.11740.

83. Trueba, F. J. & Woldringh, C. L. Changes in cell diameter during the division cycle of Escherichia coli. *J. Bacteriol.* **142**, 869–878 (1980).

84. Rowlett, V. W. & Margolin, W. 3D-SIM Super-resolution of FtsZ and Its Membrane Tethers in Escherichia coli Cells. *Biophys. J.* **107**, L17–L20 (2014).

85. Coltharp, C., Buss, J., Plumer, T. M. & Xiao, J. Defining the rate-limiting processes of bacterial cytokinesis. *Proc. Natl. Acad. Sci. U. S. A.* **113**, E1044–E1053 (2016).

86. Chen, Y. & Erickson, H. P. Rapid in vitro assembly dynamics and subunit turnover of FtsZ demonstrated by fluorescence resonance energy transfer. *J. Biol. Chem.* **280**, 22549–22554 (2005).

87. González, J. M. *et al.* Cooperative behavior of Escherichia coli cell-division protein FtsZ assembly involves the preferential cyclization of long single-stranded fibrils. *Proc. Natl. Acad. Sci.* **102**, 1895–1900 (2005).

88. GonzálezGonz, P. *et al.* Torsion and curvature of FtsZ filaments †. (2014) doi:10.1039/c3sm52516c.

89. Paez, A., Tarazona, P., Mateos-Gil, P. & Vélez, M. Self-organization of curved living polymers : FtsZ protein filaments. *Soft Matter* **5**, 2625–2637 (2009).

90. Paez, A. *et al.* Simple modeling of FtsZ polymers on flat and curved surfaces: correlation with experimental in vitro observations. *PMC Biophys. 2009 21* **2**, 1–16 (2009).

91. Márquez, I., Díaz-Haro, G. & Vélez, M. Surface Orientation and Binding Strength Modulate Shape of FtsZ on Lipid Surfaces. doi:10.3390/ijms20102545.

92. Vélez, M. How Does the Spatial Confinement of FtsZ to a Membrane Surface Affect Its Polymerization Properties and Function? *Front. Microbiol.* **13**, 757711 (2022).

93. Hörger, I., Velasco, E., Rivas, G., Vélez, M. & Tarazona, P. FtsZ Bacterial Cytoskeletal Polymers on Curved Surfaces: The Importance of Lateral Interactions. *Biophys. J.* **94**, L81–L83 (2008).

94. Krupka, M., Sobrinos-Sanguino, M., Jiménez, M., Rivas, G. & Margolin, W. Escherichia coli Zipa organizes FtsZ polymers into dynamic ring-like protofilament

structures. *MBio* **9**, (2018).

95. Loose, M. & Mitchison, T. J. The bacterial cell division proteins FtsA and FtsZ self-organize into dynamic cytoskeletal patterns. *Nat. Cell Biol.* **16**, (2014).

96. Ramirez-Diaz, D. A. *et al.* Treadmilling analysis reveals new insights into dynamic FtsZ ring architecture. *PLoS Biol.* **16**, (2018).

97. Caldas, P. *et al.* Cooperative ordering of treadmilling filaments in cytoskeletal networks of FtsZ and its crosslinker ZapA. *Nat. Commun. 2019 101* **10**, 1–13 (2019).

98. Holden, S. J. *et al.* High throughput 3D super-resolution microscopy reveals Caulobacter crescentus in vivo Z-ring organization. *Proc. Natl. Acad. Sci. U. S. A.* **111**, 4566–4571 (2014).

99. Szwedziak, P., Ghosal, D., Szwedziak, P. & Ghosal, D. FtsZ-ring Architecture and Its Control by MinCD. *Subcell. Biochem.* **84**, (2017).

100. Yao, Q. *et al.* Short FtsZ filaments can drive asymmetric cell envelope constriction at the onset of bacterial cytokinesis. *EMBO J.* **36**, 1577–1589 (2017).

101. Shtengel, G. *et al.* Interferometric fluorescent super-resolution microscopy resolves 3D cellular ultrastructure. *Proc. Natl. Acad. Sci. U. S. A.* **106**, 3125–3130 (2009).

102. Haeusser, D. P., Rowlett, V. W. & Margolin, W. A mutation in Escherichia coli ftsZ bypasses the requirement for the essential division gene zipA and confers resistance to FtsZ assembly inhibitors by stabilizing protofilament bundling. *Mol. Microbiol.* **97**, 988–1005 (2015).

103. Yang, X. *et al.* GTPase activity-coupled treadmilling of the bacterial tubulin FtsZ organizes septal cell wall synthesis. *Science (80-.).* **355**, 744–747 (2017).

104. Bisson-Filho, A. W. *et al.* Treadmilling by FtsZ filaments drives peptidoglycan synthesis and bacterial cell division. *Science (80-.).* **355**, 739–743 (2017).

105. Whitley, K. D. *et al.* FtsZ treadmilling is essential for Z-ring condensation and septal constriction initiation in Bacillus subtilis cell division. *Nat. Commun.* **12**, (2021).

106. Erickson, H. P. Modeling the physics of FtsZ assembly and force generation. *Proc. Natl. Acad. Sci.* **106**, 9238–9243 (2009).

107. Xiao, J. & Goley, E. D. Redefining the roles of the FtsZ-ring in bacterial cytokinesis. *Curr. Opin. Microbiol.* **34**, 90–96 (2016).

108. Coltharp, C. & Xiao, J. Beyond force generation: Why is a dynamic ring of FtsZ polymers essential for bacterial cytokinesis? *BioEssays* **39**, 1–11 (2017).

109. Kohyama, S., Merino-Salomón, A. & Schwille, P. In vitro assembly, positioning and contraction of a division ring in minimal cells. *Nat. Commun.* **13**, 6098 (2022).

110. Ramirez-Diaz, D. A. *et al.* FtsZ induces membrane deformations via torsional stress upon GTP hydrolysis. *Nat. Commun. 2021 121* **12**, 1–11 (2021).

111. Godino, E. *et al.* Cell-free biogenesis of bacterial division proto-rings that can constrict liposomes. *Commun. Biol. 2020 31* **3**, 1–11 (2020).

112. Hirschi, S., Ward, T. R., Meier, W. P., Müller, D. J. & Fotiadis, D. Synthetic Biology: Bottom-Up Assembly of Molecular Systems. *Chem. Rev.* (2022) doi:10.1021/ACS.CHEMREV.2C00339/ASSET/IMAGES/LARGE/CR2C00339_0015.JPEG.

113. Jiang, W. *et al.* Artificial Cells: Past, Present and Future. *ACS Nano* **16**, 15705–15733 (2022).

114. Schuck, P. Size-distribution analysis of macromolecules by sedimentation velocity ultracentrifugation and lamm equation modeling. *Biophys. J.* **78**, 1606–1619 (2000).

115. Laue, T. M., Shah, B. D., Ridgeway, T. M. & Pelletier, S. L. *Analytical ultracentrifugation in biochemistry and polymer science*. *Analytical ultracentrifugation in biochemistry and polymer science* (Royal Society of Chemistry, 1992).

116. Schuck, P. On the analysis of protein self-association by sedimentation velocity analytical ultracentrifugation. *Anal. Biochem.* **320**, 104–124 (2003).

117. Balbo, A. *et al.* Studying multiprotein complexes by multisignal sedimentation velocity analytical ultracentrifugation. *Proc. Natl. Acad. Sci. U. S. A.* **102**, 81–86 (2005).

118. Cole, J. L. Analysis of Heterogeneous Interactions. *Methods Enzymol.* **384**, 212–232 (2004).

119. Mastronarde, D. N. Automated electron microscope tomography using robust prediction of specimen movements. *J. Struct. Biol.* **152**, 36–51 (2005).

120. Zheng, S. Q. *et al.* MotionCor2: anisotropic correction of beam-induced motion for improved cryo-electron microscopy. *Nat. Methods 2017 144* **14**, 331–332 (2017).

121. Schur, F. K. M. *et al.* An atomic model of HIV-1 capsid-SP1 reveals structures regulating assembly and maturation. *Science (80-.).* **353**, 506–508 (2016).

122. Kremer, J. R., Mastronarde, D. N. & McIntosh, J. R. Computer Visualization of Three-Dimensional Image Data Using IMOD. *J. Struct. Biol.* **116**, 71–76 (1996).

123. Buchholz, T. O., Jordan, M., Pigino, G. & Jug, F. Cryo-CARE: Content-aware image restoration for cryo-transmission electron microscopy data. *Proc. - Int. Symp. Biomed. Imaging* **2019**-**April**, 502–506 (2019).

124. Goddard, T. D. *et al.* UCSF ChimeraX: Meeting modern challenges in visualization and analysis. *Protein Sci.* **27**, 14–25 (2018).

125. Pettersen, E. F. *et al.* UCSF Chimera—A visualization system for exploratory research and analysis. *J. Comput. Chem.* **25**, 1605–1612 (2004).

126. Margineanu, A. *et al.* Complexation of Lipofectamine and Cholesterol-Modified DNA Sequences Studied by Single-Molecule Fluorescence Techniques. (2007) doi:10.1021/bm700486q.

127. Pautot, S., Frisken, B. J. & Weitz, D. A. Production of unilamellar vesicles using an inverted emulsion. *Langmuir* **19**, 2870–2879 (2003).

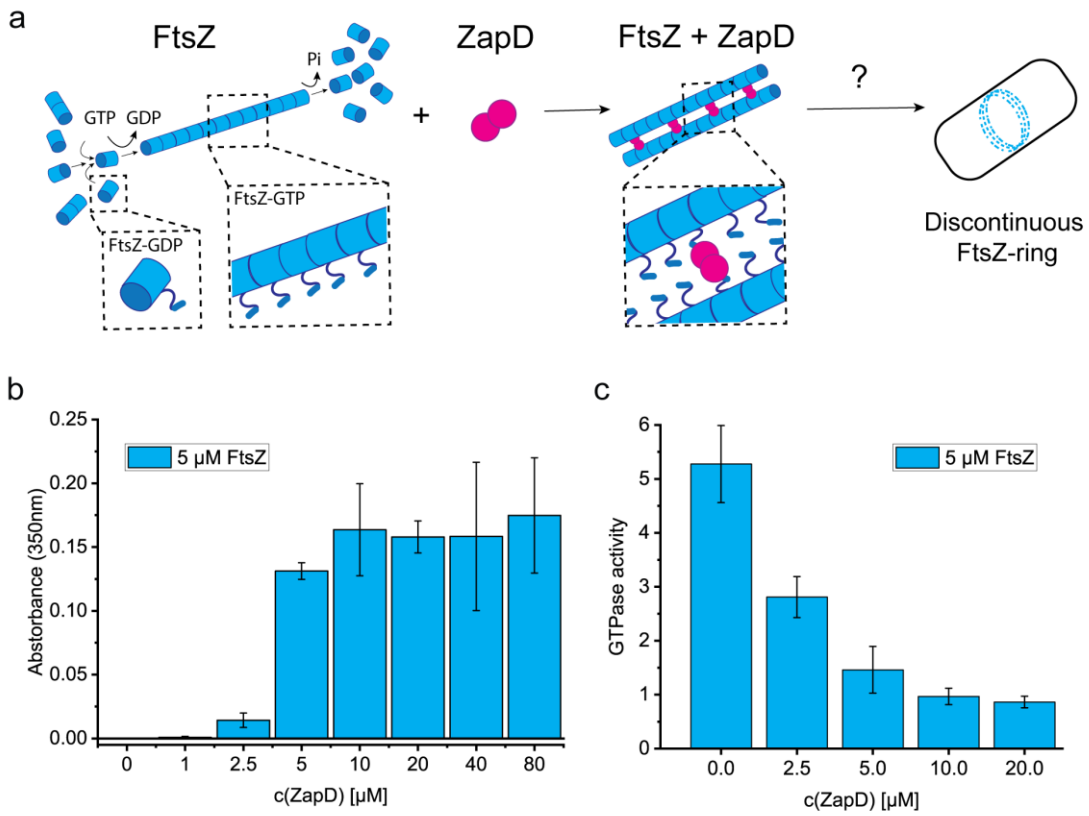

Figure 1. ZapD binds FtsZ and promotes filament bundling. **a** Scheme of the FtsZ protein and its interaction with ZapD. E. coli FtsZ (blue) forms monomers in solution that oligomerize depending on the buffer conditions. Upon GTP consumption, FtsZ homopolymerizes directionally, assembling single stranded filaments. ZapD is a robust dimer (magenta) that interacts directly with FtsZ, crosslinking filaments by promoting lateral interactions between them. Although the molecular mechanism is still unclear, the current hypothesis of interaction defines a dimer of ZapD crosslinking two FtsZ filaments through the C-terminal region of FtsZ. According to this model, the orientation of the FtsZ filaments is antiparallel, allowing the growth and treadmilling of the filaments in opposite directions. However, the mechanism of Z-ring assembly and crosslinking in the midcell is still unknown. **b** Light scattering assay measuring the absorbance at 350 nm of samples containing 5 µM FtsZ and increasing concentrations of ZapD. The light scattering of the sample was measured 5 minutes after the addition of 1 mM GTP at working buffer (50 mM KCl, 50 mM Tris-Cl, 5 mM $MgCl_2$ pH 7). FtsZ polymers do not scatter light at this wavelength; therefore, the signal at 350 nm corresponds to the presence of large FtsZ macrostructures and bundles. Blanks were measured before the addition of GTP and then subtracted from subsequent measurements. The mean value and SD of >3 independent replicates are plotted in the graph. **c** GTPase activity of FtsZ after addition of 1 mM GTP in presence of increasing concentrations of ZapD at working conditions (50 mM KCl, 50 mM Tris-Cl, 5 mM $MgCl_2$ pH 7). The mean value and SD plotted in the graph are the result of 3 independent replicates. The GTPase activity was measured as a result of the Pi released from GTP consumption. The units are Mol GTP consumed per Mol FtsZ per min.

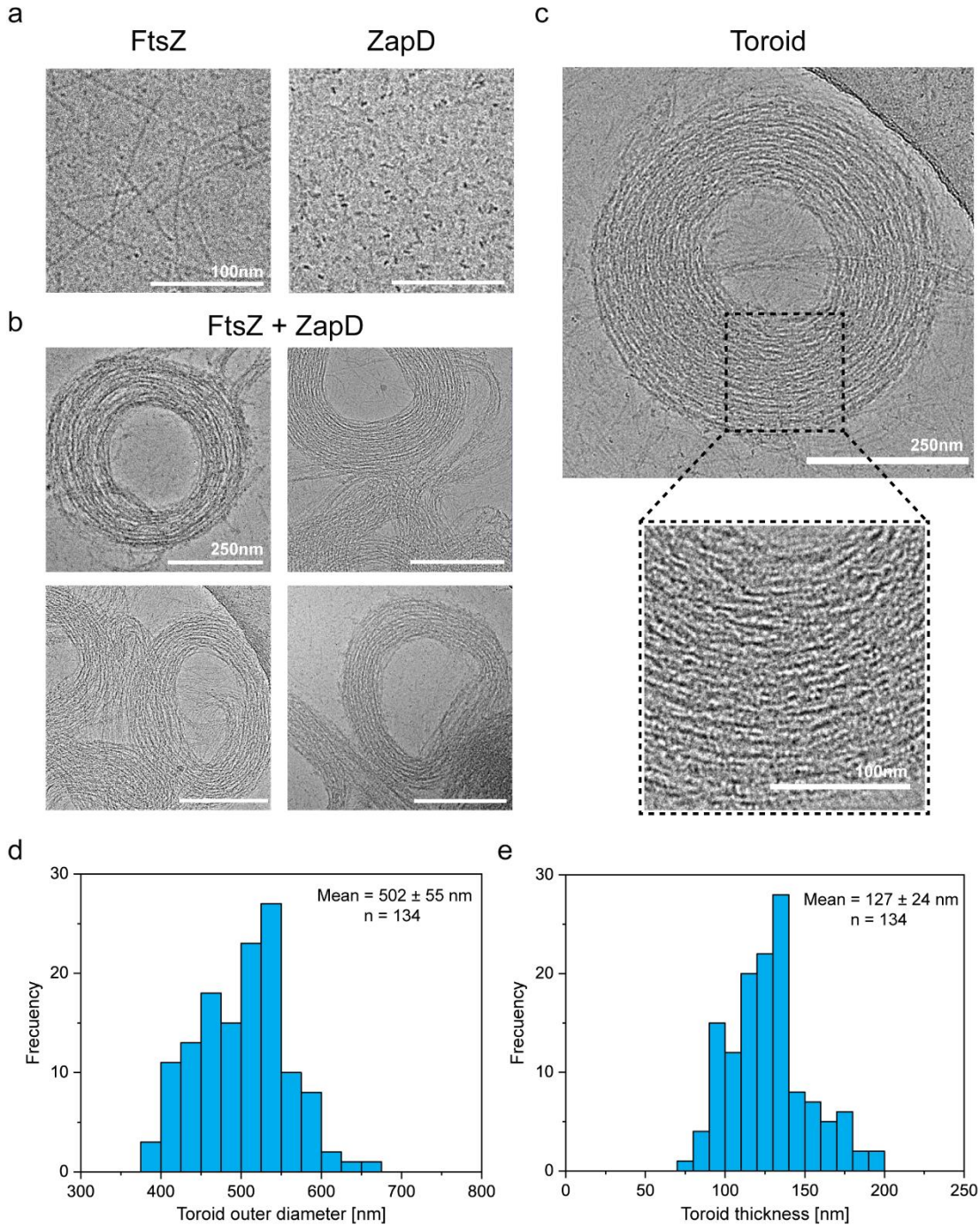

Figure 2. ZapD promotes the formation of FtsZ toroids. **a** Cryo-EM micrographs of FtsZ filaments (FtsZ-GTP form) (left) and ZapD protein (right) at 10 µM under working conditions (50 mM KCl, 50 mM Tris-Cl, 5 mM $MgCl_2$ pH 7). Scale bars are 100 nm **b** Cryo-EM images of FtsZ (10 µM) in the presence of equimolar concentrations of ZapD and 1 mM GTP in working conditions. Cryo-EM grids were plunge frozen 2 min after GTP addition to favor the assembly of FtsZ and ZapD structures. The proteins were mixed before the polymerization was triggered by GTP addition. Scale bars are 250 nm. **c** Micrograph of an individual FtsZ toroid found under the same conditions as in (**b**). Close-up view of an area within the toroid is framed by a dotted black line, revealing the large amount of FtsZ filaments that form its structure. **d** Distribution of the outer diameter of the FtsZ toroid. Each toroid was measured perpendicularly in the shortest and longest axis to ensure the reliability of the measurement. The mean value and standard deviation are shown in the graph. **e** Distribution of toroidal thickness. It was measured as the result of the difference between the outer and inner diameter of each toroid. The mean value and standard deviation are shown in the graph.

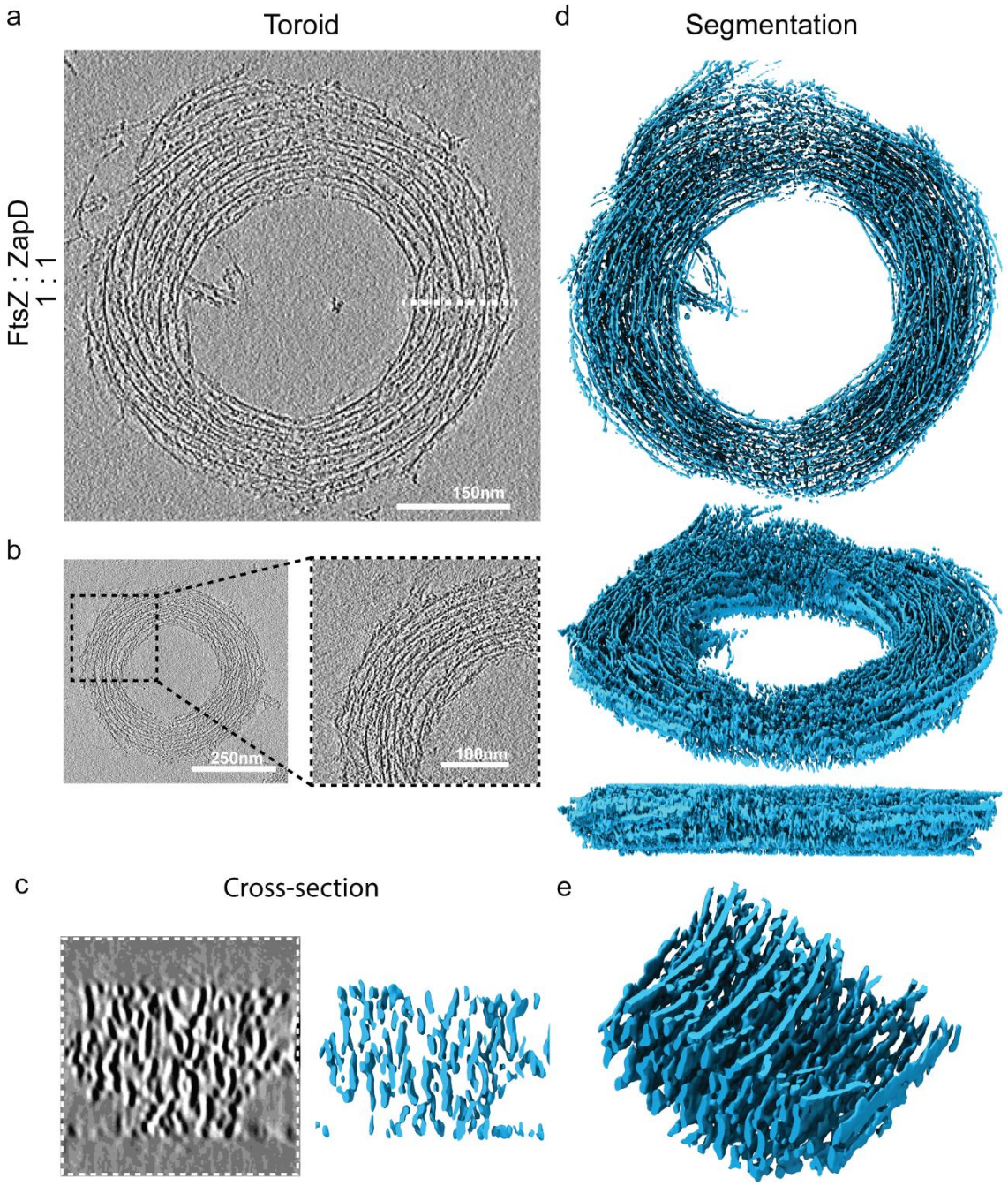

Figure 3. 3D structure of FtsZ toroids revealed by cryo-ET. **a** Representative micrograph of a FtsZ toroid resulting from the interaction of FtsZ with ZapD. The image is the average of five 6.4 nm thick tomographic slices (total thickness of 32 nm) of the reconstructed tomogram around the equatorial plane of a single FtsZ toroid. Scale bar is 150 nm. The concentrations of FtsZ and ZapD were 10 µM and 1 mM of GTP was added to trigger polymerization under working conditions (50 mM KCl, 50 mM Tris-Cl, 5 mM $MgCl_2$ pH 7). **b** Cryo-ET image of a single FtsZ toroid. A close-up view of the toroidal structure (left) shows the alignment of FtsZ filaments forming the toroid. The image is the average of five tomographic slices of the reconstructed tomogram. 10 µM FtsZ was used with either equimolar or double (20 µM) concentration of ZapD in the presence of 1 mM GTP. No significant structural differences were observed in the toroidal structures among samples containing equimolar or double ZapD concentrations**. c** Cryo-ET image (left) shows the cross-section corresponding to the area located at the white dotted line in **(a).** This image is the average of nine tomographic slices from the denoised tomogram. The isosurface of the cross-section (right) shows the alignment

and organization of the FtsZ filaments within the toroid. This suggests a regular distribution of filaments assembling the toroid. FtsZ filaments are represented in blue. **d** Isosurface of the FtsZ toroid shown in (**a**). It was extracted from the reconstruction of the denoised tomographic volume and positioned in different views to facilitate its visualization: (top) front view, (middle) side view and (bottom) lateral view. **e** A close-up view of the segmented toroidal structure. It shows the complex internal organization of filaments assembling the toroid. It corresponds to a zone within the toroid shown in **(d)**.

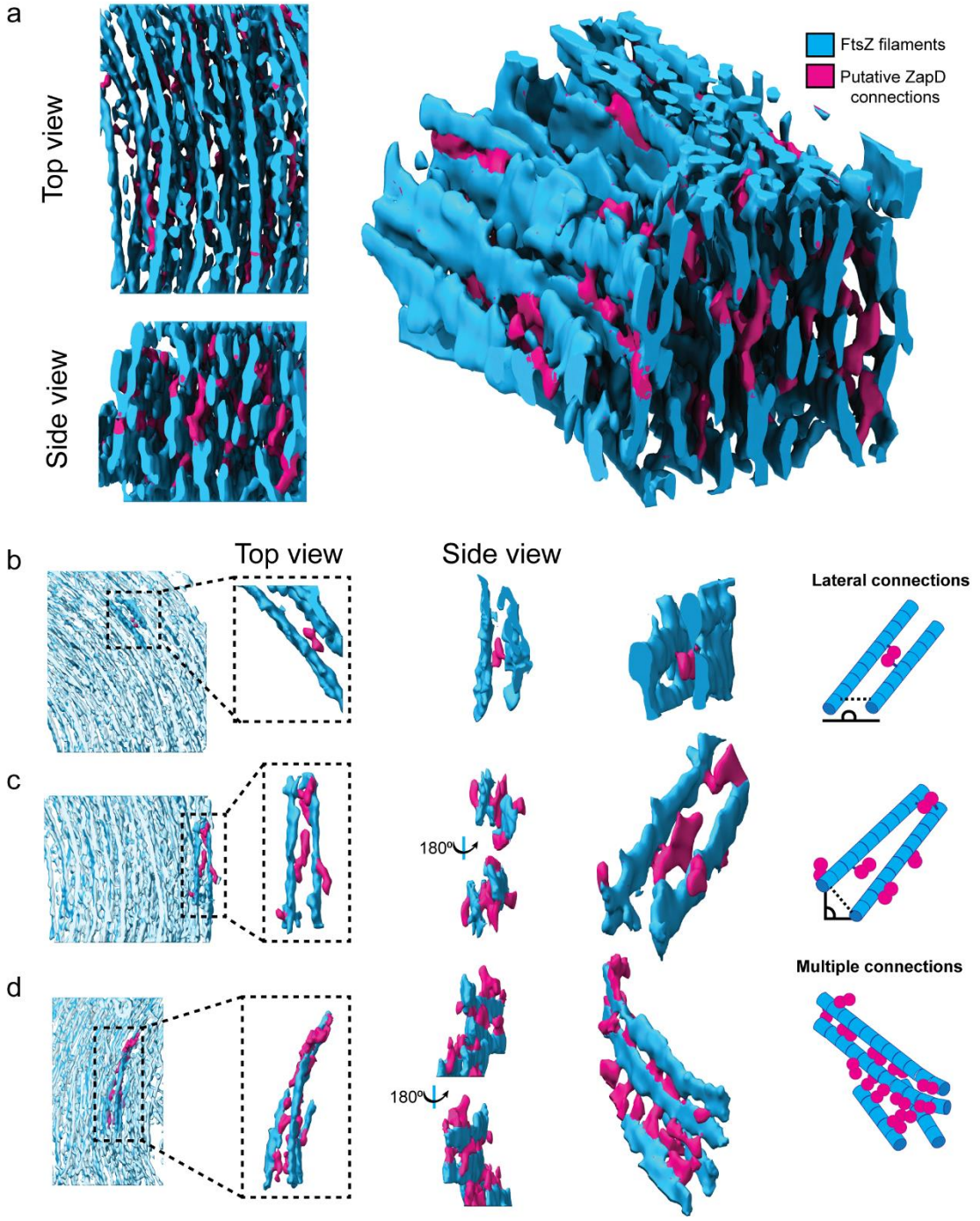

Figure 4. FtsZ filaments are connected by putative ZapD crosslinkers to assemble the toroidal structure. **a** Top (left, top), side (left, bottom) and lateral (right) views of the isosurface from an area within the toroidal structure shown in (Fig. 3a). The FtsZ filaments are colored blue, while filament connections or putative ZapD proteins are labelled magenta to facilitate interpretation of the results. Other putative ZapD proteins decorating the FtsZ filaments were not labelled in magenta because they were not forming any clear connection between the filaments. **b-d** Different examples of connections between filaments by putative ZapD proteins within the toroid. Filaments are labelled in blue and putative ZapD in magenta to facilitate their interpretation. From left to right, the localization of the analyzed area, a close-up view of the structure of interest, different views of the connections and a schematic to illustrate the interpretation of the data. The schematic (right) represents the localization of ZapD proteins (magenta) and FtsZ filaments (blue). **b** Lateral connection of two FtsZ filaments by a putative ZapD dimer. In this example, the attachment of each globular density or putative ZapD

monomer was bound to each filament, allowing for a lateral connection **c** Putative ZapD connections stabilizing two filaments by a lateral interaction. Additional ZapD decorations attached only to one of the filaments appear to be available for other connections. **d** Multiple ZapD proteins can connect to filaments and stabilize the interaction. First, the two upper filaments are connected to each other by lateral connections through several putative ZapD. The lower filament connects laterally with the two other filaments. In the upper part, additional decorations or putative ZapD proteins would be available to establish further connections forming a tridimensional mesh.

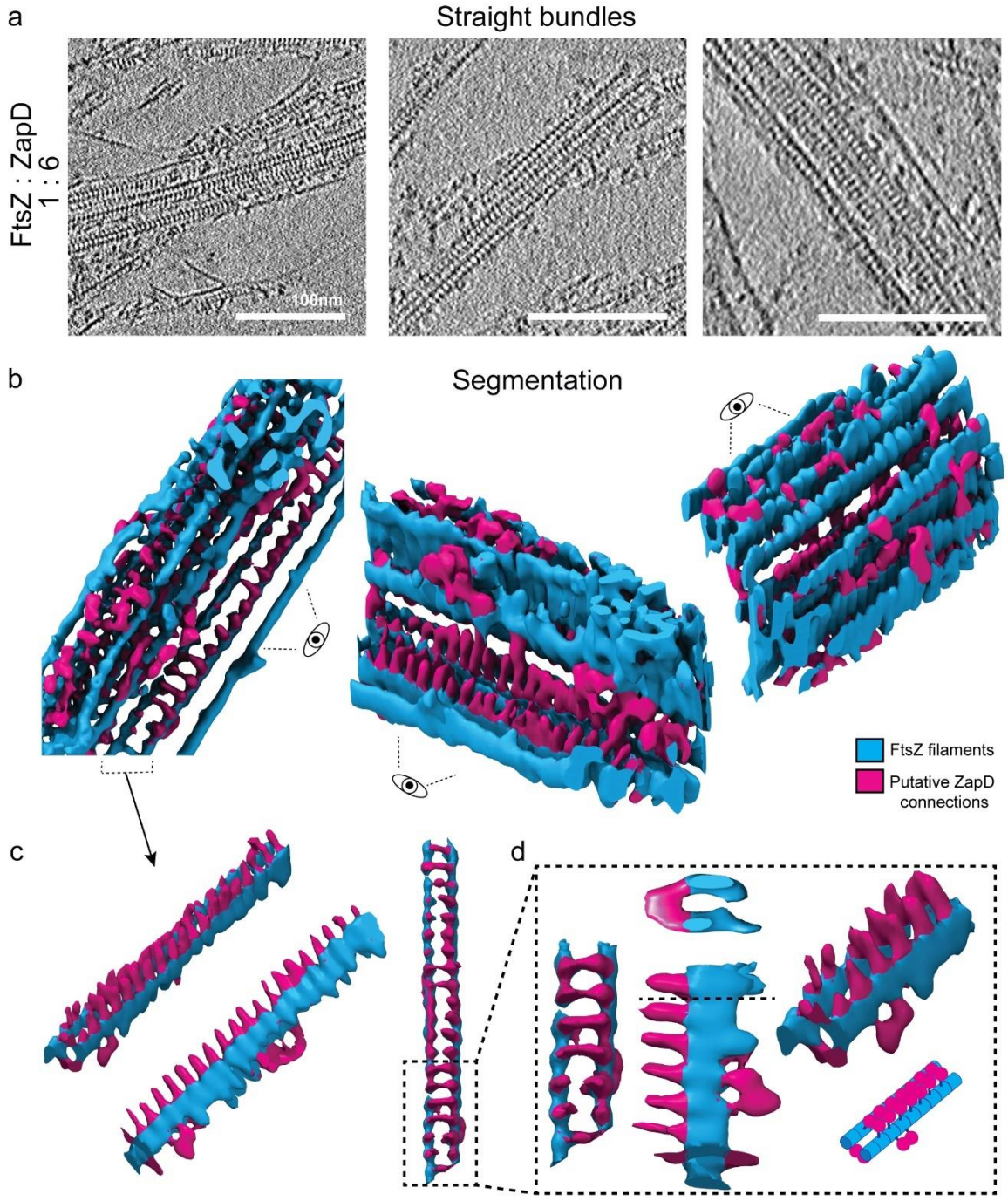

Figure 5. The presence of a high ZapD concentration promotes the formation of straight FtsZ bundles. **a** Representative images of straight FtsZ bundles resulting from the interaction of FtsZ with high ZapD concentrations under working conditions (50 mM KCl, 50 mM Tris-Cl, 5 mM $MgCl_2$ pH 7). The concentrations of FtsZ and ZapD were 10 µM and 60 µM, respectively, and 1 mM of GTP was added to trigger polymerization. The straight bundles were only found at high ZapD concentrations. The image is the average of five 6.4 nm thick tomographic slices (total thickness of 32 nm) of the reconstructed tomogram. Scale bars are 100 nm. **b** Isosurface of the straight bundles from the denoised tomographic volume. FtsZ filaments are colored in blue and putative ZapD connections in magenta. Three different views (top (left) and side views (middle, right)) are shown. Straight bundles are organized in a regular organization. Multiple connections between filaments are found in a very regular manner; putative ZapD proteins align and stack to stabilize two FtsZ filaments by crosslinking them. In addition, lateral

connections were also found linking couple of stabilized filaments among them, ultimately assembling the straight bundle. **c** Different views of one of the isolated filaments from the straight bundle. A side view of the filaments (middle) shows a spike-like structure regularly located at the top of the FtsZ filaments, connecting them as observed in the top view (right). **d** Different close-up views of the filament structure shown in **(c).** In the cross-section of the structure (middle, top), it is clearly visible that the ZapD proteins connect the two filaments, forming a bridge over them. A schematic of the suggested interaction (right, bottom) shows the location of putative ZapD dimer in this structure.

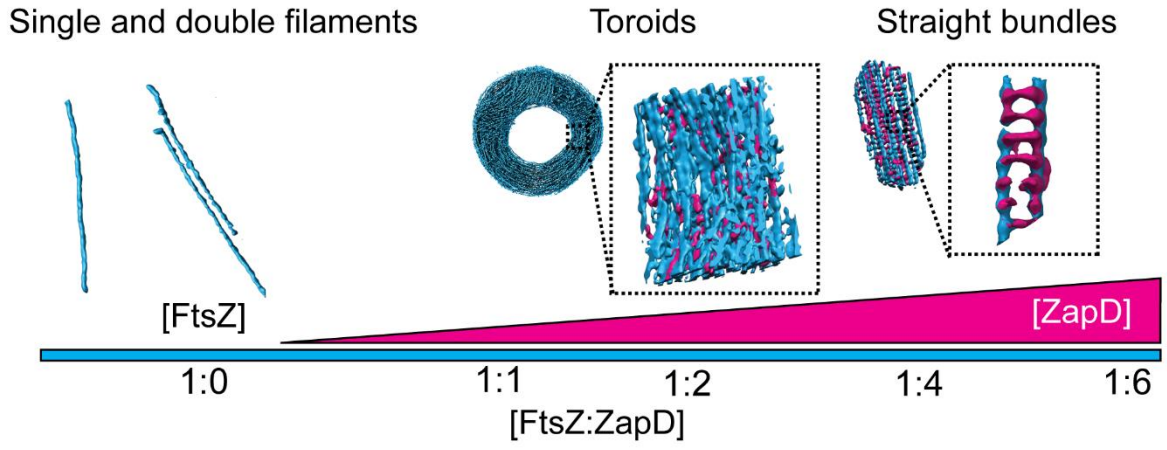

Figure 6. Proposed molecular mechanism of the bundling effect of ZapD on FtsZ filaments. Based on our experiments and in agreement with preliminary studies, we propose a molecular mechanism for the interaction between FtsZ and ZapD. FtsZ filaments are highly dynamic and they can interact laterally with each other, forming double filaments through weak lateral interactions. On the other hand, each ZapD dimer can bind to two FtsZ filaments, promoting the formation of lateral interactions between FtsZ filaments. At low concentrations of ZapD, only a few lateral connections are formed and thus no bundles can be assembled. However, at higher ZapD concentrations, reaching a protein ratio of FtsZ and ZapD of 1:1 or 1:2 (FtsZ:ZapD), more ZapD-mediated connections are established between FtsZ filaments and the formation of bundles and toroidal structures is favored. Toroidal structures are composed of a meshwork of short filaments, crosslinked laterally by ZapD dimers. A further increase in the concentration of ZapD (protein ratio of 1:4 or 1:6 (FtsZ:ZapD)) can also increase the number of connections on the FtsZ filaments, straighten up their structure and allowing the formation of straight bundles. This structure is formed only under high ZapD concentrations although coexists with scarce toroidal structures. The assembly of FtsZ macrostructures is dependent on the number of lateral connections through ZapD dimers and some intermediate states are expected between toroids and straight bundles.